New Tools for Terrain Gravimetry
NEWTON-g
Project number: 801221

Deliverable 4.1

Parameters definition for devices design

Lead beneficiary:	Helmholtz-Zentrum Potsdam. Deutsches GeoForschungsZentrum (GFZ)
Dissemination level:	Public
Version:	Final

NEWTON-g has received funding from the EC's Horizon 2020 programme, under the FETOPEN-2016/2017 call (Grant Agreement No 801221)

Document Information

Grant Agreement Number	801221
Acronym	NEWTON-g
Start date of the project	1 June 2018
Project duration (months)	48
Deliverable number	D4.1
Deliverable Title	Parameters definition for devices design
Due date of deliverable	30 September 2018
Actual submission date	05 October 2018
Lead Beneficiary	GFZ
Type	R: Document, report
Dissemination level	PU - Public
Work Package	WP4 - Data analysis

Version	**Date**	**Author**	**Comments**
v.0	27 September 2018	Nikkhoo, Rivalta, Carbone	Creation
v.1	02 October 2018	Busquet, Lautier-Gaud	Revision
v.2	03 October 2018	Middlemiss, de Zeeuw - van Dalfsen	Revision
Final	05 October 2018	Nikkhoo, Carbone	Validation

TABLE OF CONTENT

1. INTRODUCTION

The main objective of NEWTON-g is the development of a *gravity imager* including MEMS (Microelectromechanical System) *pixels* anchored to a reference absolute gravimeter, the latter based on quantum technology. Once developed, this system for dense gravity measurements will be field-tested at Mt. Etna volcano, in order to check its performance under harsh out-of-the-lab conditions. The present document is meant to provide information on some key characteristics (magnitude, time-scale, wavelength) of the gravity changes expected to occur in volcanic areas (with special focus on Etna), due to underground mass redistribution triggered by both volcanic and hydrological processes.
The final sections describe (i) how the environmental parameter that mostly affects the performances of gravimeters, namely, ambient temperature, varies in the summit zone of Etna over different time scales (daily to seasonal) and (ii) how volcanic tremor affects standard gravimeters.

2. TIME SCALE, WAVELENGTH AND MAGNITUDE OF VOLCANO-RELATED GRAVITY CHANGES

Gravity measurements have proven essential to detect subsurface mass redistributions at active volcanoes and provide constraints on the nature of the transferred masses (Carbone et al., 2017, Segall 2010, Battaglia et al., 2003). NEWTON-g proposes to develop a *gravity imager*, namely an array of gravimeters, aiming at continuously recording 2D *images* of the gravity field over the summit zone of Mt. Etna volcano. In analogy with optics, key characteristics of the imager are the size of the pixels, the size and the shape of the array of pixels, and the self-noise of the pixels. It is thus important to match the key characteristics of the gravity imaging system to the key parameters of the gravity changes driven by volcanic and hydrological processes. In other words, the ability to detect a given gravity change depends on the spatial resolution and extent of the gravity network and the resolution of the gravity measurements, and designing an optimal system to observe gravity changes demands an overview of the expected amplitudes, time scales and wavelengths of the gravity changes associated with various source processes.
Volcanic processes able to induce important bulk mass redistribution (see also Carbone et al., 2017) include emplacement of dikes, formation of eruptive fissures and lava flows (Branca et al., 2003, Carbone et al., 2008a), shallow processes leading to lava fountaining (Carbone et al., 2015), accumulation and discharge of magmas at a reservoir (Carbone et al., 2003), redistribution of magmas through convective flows in reservoirs and lava lakes (Carbone and Poland 2012), segregation of bubbles and out-gassing through eruptive vents (Carbone et al., 2008b), volcanic earthquakes, rifting (Branca et al., 2003) and caldera collapse (Furuya et al., 2003a; 2003b).
The diagram in Fig. 1 illustrates the typical ranges of time scales and amplitudes of gravity variations associated with a number of common volcanic processes. The characteristics of the gravity change associated with each process are compiled based on different observations conducted during the past few decades, through both continuous and campaign measurements,(see Carbone et al., 2017 and references therein). In all cases,

the gravity measurements were conducted at safe distances from the hazardous processes, such as lava fountains. It is likely that higher amplitudes would be recorded at closer distances from the active structures, but this cannot be achieved with the currently available instruments.

Most processes illustrated in Fig. 1 are directly linked to fluid transport:

Magma intrusions, or dikes, are common phenomena at volcanoes. They involve the ascent or lateral transport of magma from a source (reservoir) in the form of a "blade" or "sheet" that makes its way through the Earth's crust by fracturing the rock at its tipline. The typical dimensions of a dike intrusion at Etna are a thickness of 30cm to a few meters, and a length and a height of a few hundreds of meters to a few kilometers, although at other volcanoes dikes can be larger than this. Typical dike volumes at Etna are $\sim 10^7$ m^3. Dikes at shallow crustal depth propagate at the speed of people walking, that is, on the order of 1-4 km h^{-1}. They can get arrested at depth or can propagate up to the surface and create an eruptive fissure. The spatial distribution of eruptive fissures at Etna is shown in Fig. 2.

Changes in the fracturing rate may be triggered by dikes that almost reach the surface, due to the strong deformation they induce on the Earth's surface, and by larger-scale changes in the stress field acting on the volcano. A few gravity records can unequivocally be ascribed to this. For example, Branca et al (2003) interpreted a gravity decrease prior to the 2002 NE Rift eruption at Etna as due to the opening of a shallow fracture system. Using data acquired at Etna between 1994 and 2001, Carbone et al (2009, 2014) found a marked coupling between gravity changes and release of seismic energy over both time and space and proposed that the observed gravity anomalies reflected changes in the rate of micro-fracturing along the NNW-SSE fracture/weakness zone that crosses the SE slope of Etna.

Shallow magma transport takes often a different form due to the lower confining pressure that allows for the existence of open conduits at the volcano summit. At Etna, through the summit conduits, the shallow magma chambers feed Strombolian activity (explosions connected with the transport of large gas bubbles through the conduit) or lava fountains. Typical duration of lava fountains at Etna is from a few hours to a few days.

Magma storage occurs at magma chambers, or magma reservoirs. Note that these two words are often used interchangeably, but some scientists differentiate between them: a magma chamber is intended as the storage zone of eruptible, predominantly molten magma (melt >50%), while a magma reservoir is a wider storage zone, including a so-called crystal mush, containing more or less interconnected crystals with some melt filling pore space. Both magma chambers and reservoirs vary widely in shape and size across different volcanoes. At Etna magma storage is probably articulated in more than one magma reservoir. They are not thought to be very large, roughly a few km^3. At other volcanoes, e.g. calderas, such as Campi Flegrei or Yellowstone, magma reservoirs are orders of magnitude larger than this. Processes thought to occur at magma chambers include bubble formation, crystallization, segregation of bubbles into foams, intrusion of new magma from below, convection, etc. Those involving the formation and segregation of gases may be those causing the largest gravity signals, due to the high density contrast between bubble-rich and bubble-poor magma.

Lava lakes fill the summit craters of a few volcanoes around the world (Etna is not among them). The lava lakes may experience periodic overturn, convection, phase transitions, etc.

Caldera collapse occurs when a magma chamber is drained very effectively and its roof slips on ring faults. The time span indicated in Fig. 1 corresponds approximately to the onset of the main (or first) collapse event. Further stages of a caldera collapse are expected to change the gravity to a much lesser extent but they may continue for several months. Caldera collapse has never occurred in historical time at Etna.

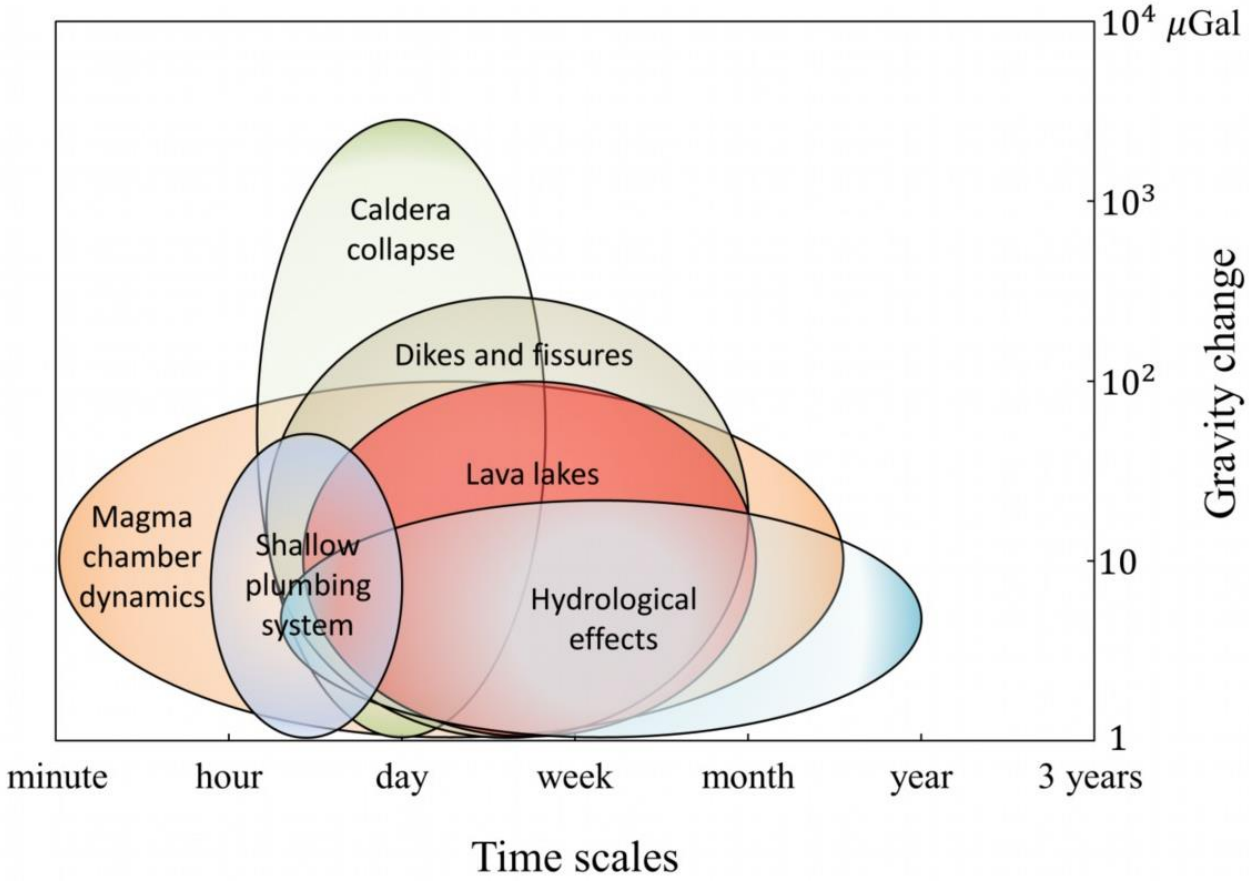

Figure 1: Amplitude of observed gravity variations, due to volcanic processes, versus their time scales. Hydrological effects (see Section 3) are also reported for the sake of comparison.

The diagram in Fig. 3 depicts the ranges of spatial wavelengths for gravity anomalies driven by common volcanic processes at Mt. Etna (Carbone at al., 2003, Branca et al., 2003, Carbone et al., 2008a, Carbone et al., 2015 and Carbone et al., 2017). Magma chamber dynamics are capable of producing gravity change with the largest wavelengths. The depths of inferred shallow and deep magma reservoirs at Mt. Etna vary in a range of 1 to 9 km below the summit, corresponding to the range from 2 km above sea level to 6 km below sea level (Budetta et al., 1999, Carbone et al., 2003, Bonforte et al., 2008, Carbone et al., 2009, and Carbone et al., 2014). The wavelengths of gravity change produced by magma chamber dynamics at these depths may reach to up to ~20 km. This estimate is supported by the gravity surveys conducted along two profiles in the Etna gravity network, which revealed gravity changes with wavelengths of up to 8 km (Budetta et al., 1999) and 15 km (Carbone et al., 2003).

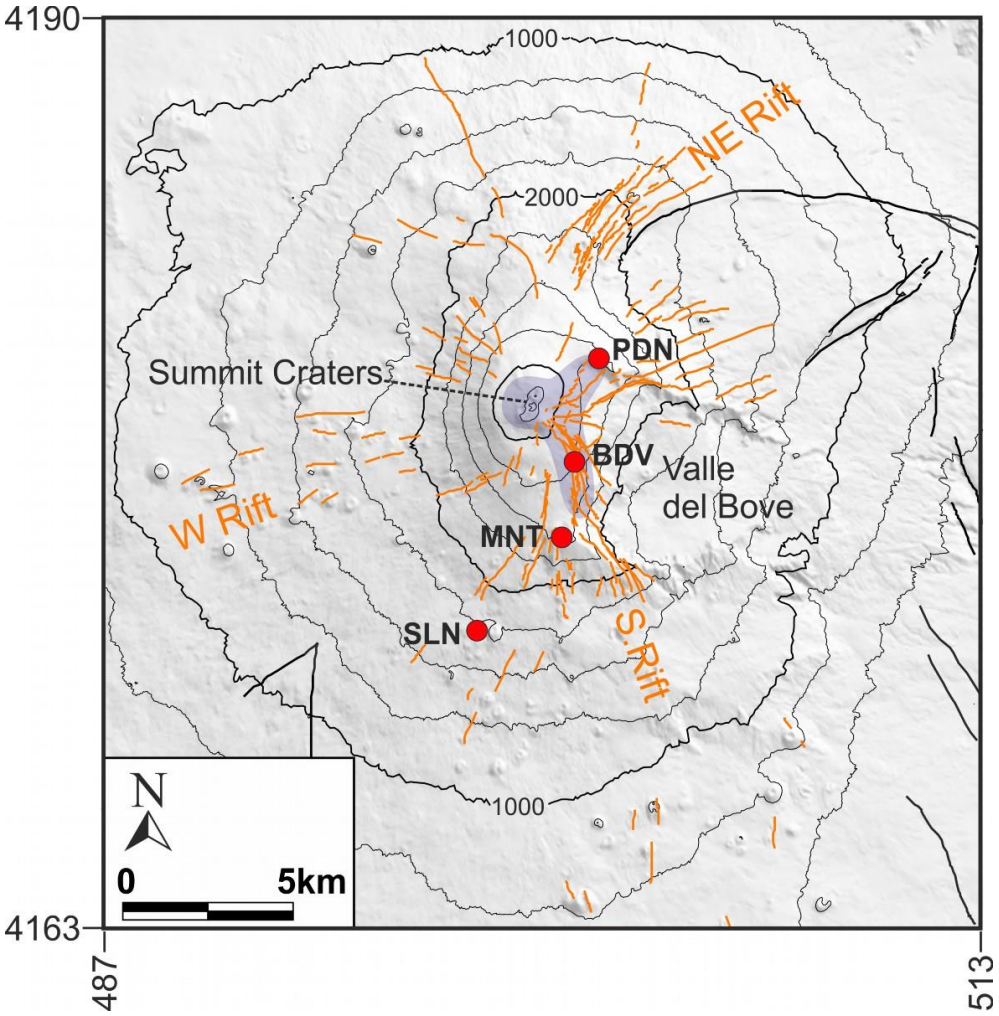

Figure 2: Sketch map of Mt. Etna showing position of the Summit Craters, main eruptive fissure systems (orange lines) and gravity stations for continuous measurements (red dots) referred to throughout the text. The shaded blue area encloses the horizontal locations of the gravity sources identified by past studies.

Considering the inferred source depths for the lava fountains at Mt. Etna, this process is expected to produce gravity anomalies with wavelengths on the order of 4 to 6 km. Similar analyses for dikes and eruptive fissures, based on their inferred dimensions at Mt. Etna, suggest that they are capable of producing gravity change signals with wavelengths of up to 10 km.

Based on these observations and analyses and considering the spatial distribution of eruptive fissures and summit craters illustrated in Fig. 2, an inter-node distance on the order of 0.5 to 1 km seems adequate to properly observe the expected gravity variations in the summit zone of Mt. Etna. The overall size of the gravity imager that will be developed under NEWTON-g will determine the upper limit of the wavelength of the observable gravity variations.

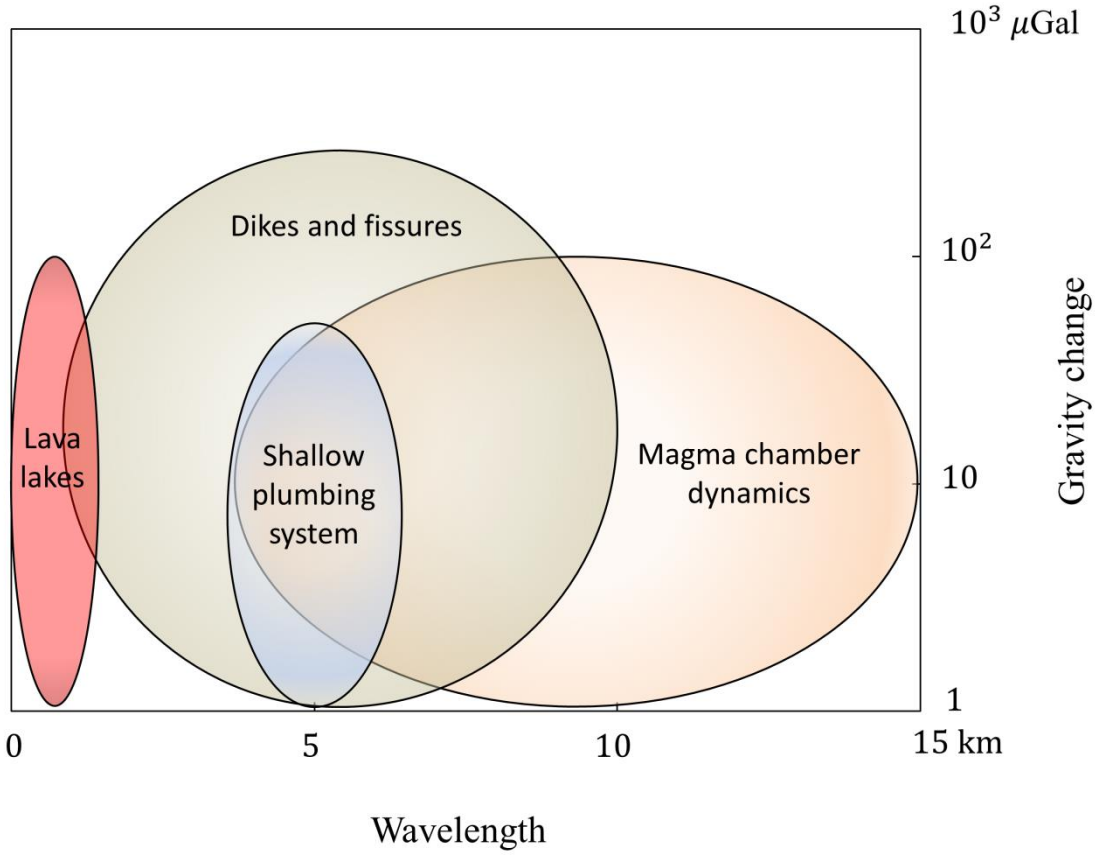

Figure 3: Amplitude of gravity variations observed at Mt. Etna versus their spatial wavelengths. See text for further details.

3. CHARACTERISTICS OF THE GRAVITY CHANGES DRIVEN BY HYDROLOGICAL PROCESSES

Changes in groundwater mass may induce gravity changes measurable at the surface, over a wide range of time scales (hours to years; Creutzfeldt et al., 2008). Hemmings et al (2016) showed that this effect can reach a few to a few tens of μGal, with higher values (>100 μGal) occurring under tropical climates.

At a given observation point, the gravity effect due to changes in the underground water-mass depends on several overlapping components, including precipitation (both rainfall and snowfall), evapotraspiration and water runoff from the storage volume beneath the installation site.

Beside water table fluctuations, shallower water-mass changes, i.e., occurring within the vadose zone, can induce measurable gravity fluctuations. In areas where the vadose zone is relatively thick, most of the water-related gravity effect may come from water-mass changes in the unsaturated zone above the water-table.

Assuming that the changes in underground water-mass are mostly seasonal and consistent, Carbone et al (2003) estimated the gravity effect of water-mass fluctuations at Mt. Etna by band-pass filtering (cut-off periods centered around 1 yr) the averaged gravity data from all the stations of the EW profile, during a 5-year interval (1994-99). The latter

profile includes about 20 stations in the southern slope of the volcano and covers a distance of 25 km, at elevations between about 500 and 2000 m. Results (Fig. 4) indicate that the **almost seasonal hydrologically induced gravity fluctuation has a maximum peak-to-peak amplitude of ~20 µGal**.

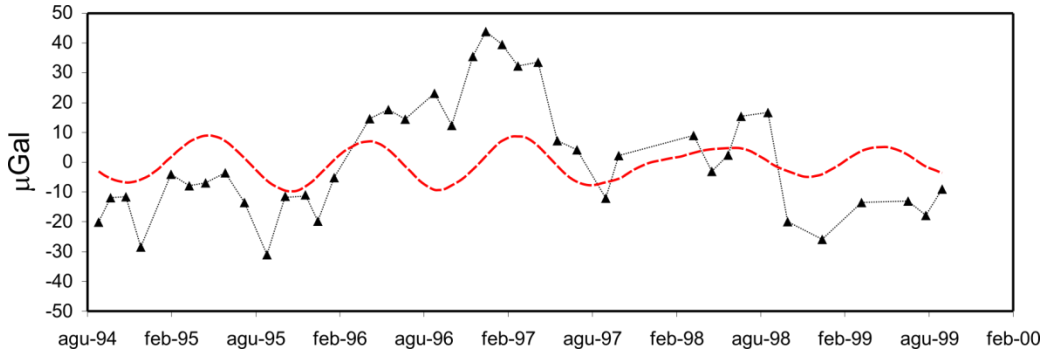

Figure 4 - Model for the gravity effect of groundwater mass fluctuation (red dashed line), obtained through a bandpass filter (cut-off periods centered around 1 yr) over the averaged data from the EW profile (black triangles), during a 5-year interval. Figure adapted from Carbone et al. (2003).

Under some conditions, the gravity effect of inter-annual water-mass fluctuations may dominate over seasonal cycles, implying that campaign measurements (usually repeated every few month to years) are, in general, not well-suited to study gravity changes due to hydrological processes. Indeed, continuously recording instruments, supplying data of adequate quality, are needed to thoughtfully address these issues. At Mt. Etna, the employment of superconducting gravimeters (SGs) since 2014 has allowed the collection of long time-series featuring very high precision and long-term stability. In particular, a 3-year dataset of continuous gravity observations, collected through a SG installed at SLN station (Fig. 3; 1730 m a.s.l), allowed a precise definition of the gravity effect induced by underground water-mass changes. The model of water-related gravity changes (Fig. 5a) was obtained following the empirical method of Crossley et al (1998) and using (i) snowfall data (Fig. 5b), evaluated through GNSS reflectometry on the signal from a GPS station only 30 m from the installation site of the SG and (ii) rainfall data (Fig. 5c) from the meteorological station managed by the Astrophysical Observatory of Serra La Nave (Italian National Institute of Astrophysics). Results show that, during the studied interval, **rainfall drove only a minor component of the total groundwater-induced gravity effect (up to 10-15 µGal peak-to-peak)**, while rapid increases in groundwater mass, during **phases of snow melting resulted in stronger gravity effects (up to 20 µGal over intervals of ~2 months)**. It is worth noting that since topography in the surroundings of the installation site is almost flat, snow accumulation occurs on the same horizon as the observation point, implying a negligible effect on the vertical component of the gravity acceleration; conversely, snow melting induces a rapid increase of the groundwater mass, resulting in a measurable gravity change.

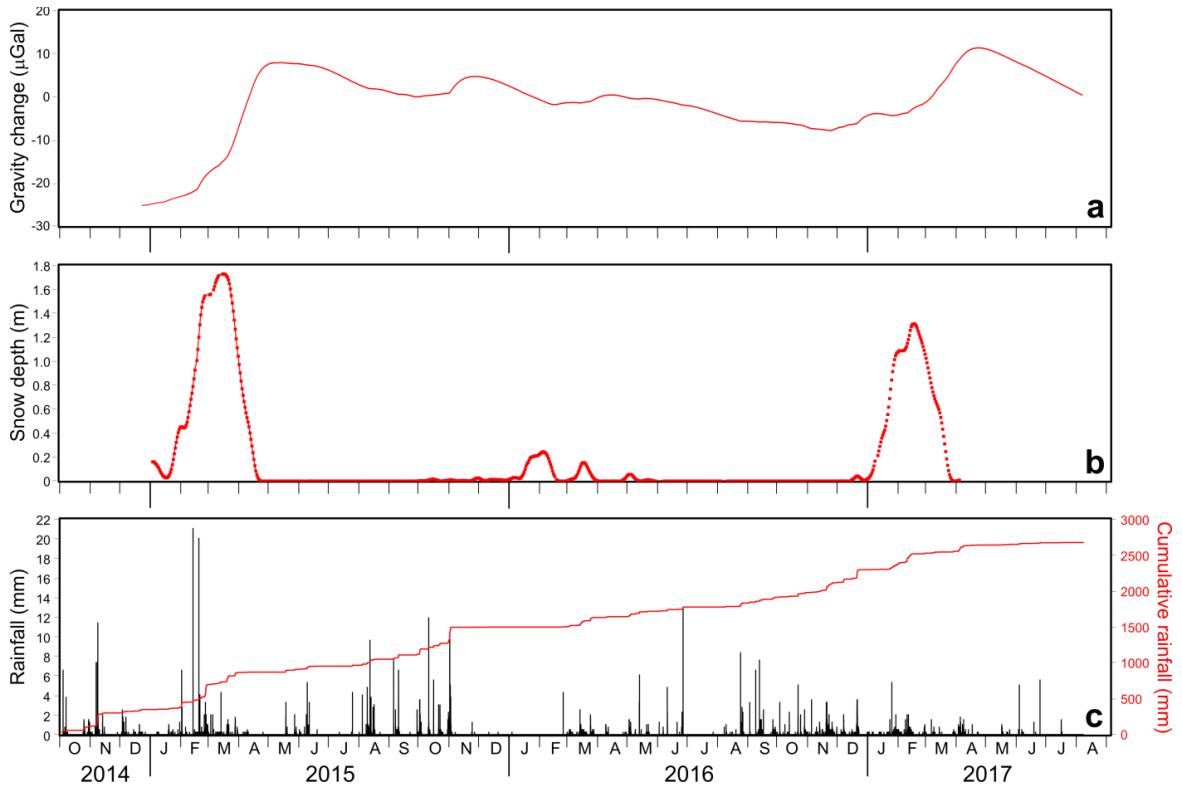

Figure 5 - (a) Model of the gravity changes induced by groundwater mass changes at SLN between late 2014 and early 2017. (b) Snow depth evaluated through GNSS reflectometry at SLN. (c) Time series of rainfall data from SLN.

In the time-series from another SG installed at MNT (Fig. 3; 2600 m a.s.l.), **sudden changes (over periods of a few hours to a few days) were observed, with amplitude within 10 µGal, that took place simultaneously with rainfall events**. At SLN the same rainfall events are associated with either no change, or changes with amplitude much lower than at MNT. These observations suggest that similar patterns of hydrological input (the two sites are less than 4 km apart) induce different gravity responses at SNL and MNT, due to site effects: at MNT the gravity effect of water content variations in the shallowest ash layers beneath the observation point dominates over the effect of hydrogeological processes at greater depth, due to structural and topographic constraints.
In conclusion, the above observations indicate that, at Mt. Etna, hydrological processes may induce measurable gravity changes over a **wide range of time-scales, from hourly to seasonal**. The **amplitude of these changes varies from a few to few tens of µGal** (see Fig. 1).

4. VARIABILITY RANGES OF AMBIENT TEMPERATURE AT Mt. ETNA

Past studies have shown that ambient temperature affects the signal from standard gravimeters, especially when they are used as continuously recording devices (Andò and Carbone, 2004; 2006). The instruments that will be developed in the framework of NEWTON-g may also be influenced by changes in ambient temperature. As for quantum

gravimeters, changes in ambient temperature greatly affect the performance of the optical components used to perform the measurement, hence affecting the stability and the resolution of the gravity measurement (Menoret et al., 2018). The MEMS gravimeter (if not temperature controlled) would measure spurious signals associated with the change in Young's modulus – and therefore spring constant – of its silicon flexures (Middlemiss et al., 2017). It is thus important that the design of these instruments takes into account the variability ranges of ambient temperature expected at the field test site, i.e., at Mt. Etna.
External ambient temperature data recorded at SLN (Fig. 3) during a 3-year interval are shown in Fig. 6.

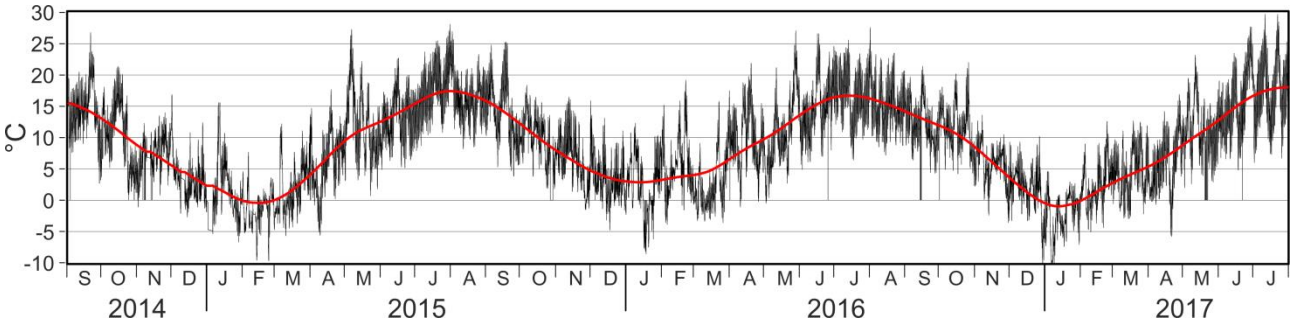

Figure 6 - External ambient temperature measured at SLN during September 2014 to July 2017. The red curve is a low-pass filter (cut-off period ~120 days), aimed at evidencing the seasonal component of the signal.

The peak-to-peak amplitude of the seasonal component (red curve in Fig. 6) is within 20°C. However, due to shorter-period components superimposed on the seasonal one (mostly, daily fluctuations), the overall peak-to-peak amplitude is about 30°C. Indeed, the daily fluctuation amounts to up to 10°C (Fig. 7), while changes with period of 10-20 days can reach amplitudes of 20°C.

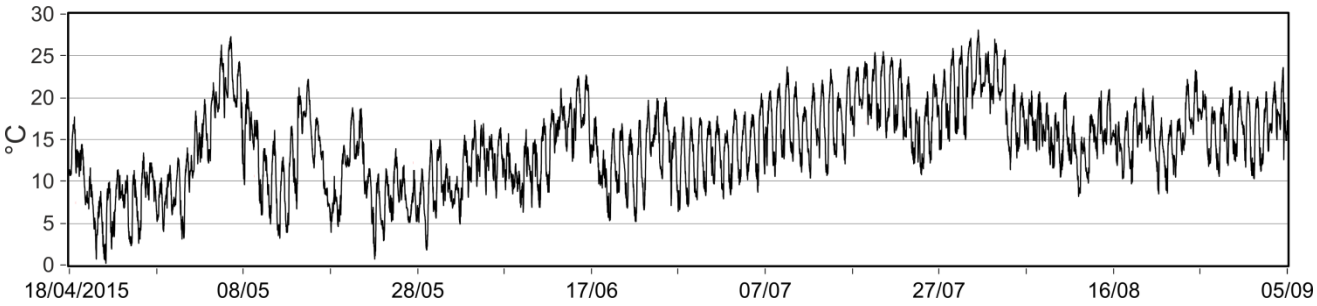

Figure 7 - 140-day sub-interval of the time series shown in Figure 6.

External ambient temperature data are not available for sites on Etna at higher elevation than SLN. However, ambient temperature is usually recorded inside the infrastructures (semi-underground concrete boxes; Fig. 8) hosting continuously recording gravimeters in the summit zone of Etna. In most cases, ambient temperature is recorded both inside and outside the inner polyurethane box that further protects the gravimeter from temperature changes (Fig. 8). Since the MEMS sensors that constitute the *pixels* of the *gravity imager*

will be installed inside similar containers, it is important to consider previous ambient temperature data collected at continuously recording gravity stations in the Etna's network. One of the longest lasting uninterrupted time sequences of internal ambient temperature comes from BVD station (Fig. 3; 2860 m elevation) and is shown in Fig. 9 (more than 1 year of data, from late 2004 to early 2006). The thermometers utilized to collect this dataset are not able to record negative temperatures. However, as shown in Fig. 9, the latter occur only rather rarely outside and never inside the inner polyurethane box.

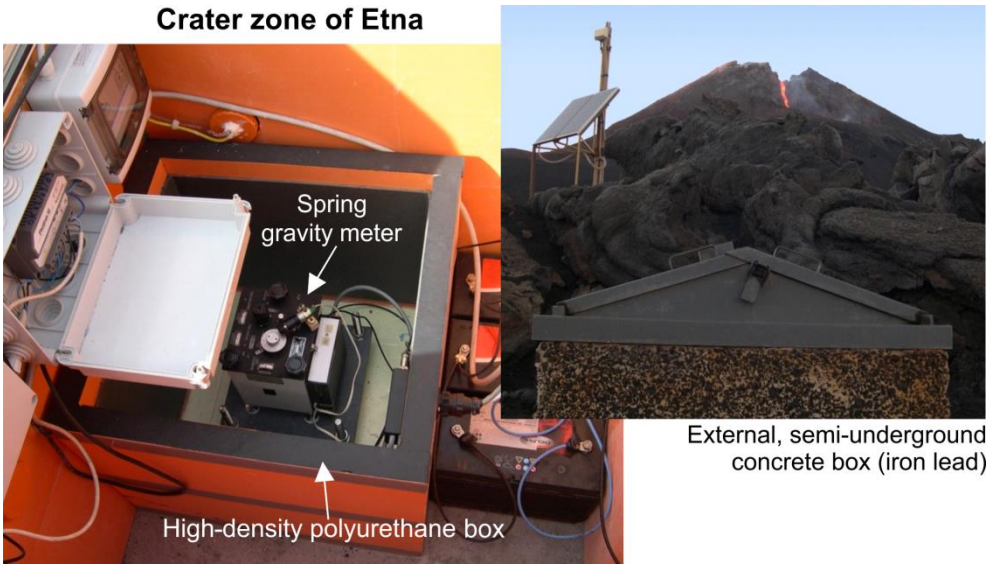

Figure 8 - Setup of a gravity station in the summit of Etna (station BVD; Fig. 3). The gravimeter, inside the semi-underground concrete box (on the right, with erupting crater in the background), is protected by a thermally insulating polyurethane box (left).

Outside the polyurethane box the seasonal component has a peak-to-peak amplitude of 15 to 20°C, while the overall peak-to-peak amplitude is >25°C, due to the presence of important shorter period components, mostly daily (peak-to-peak amplitude of the daily component is up to 10°C; Fig. 10). The inner polyurethane box efficiently reduces the peak-to-peak amplitude of both seasonal and daily components to about 10 (6 to 16°C) and 2°C, respectively.

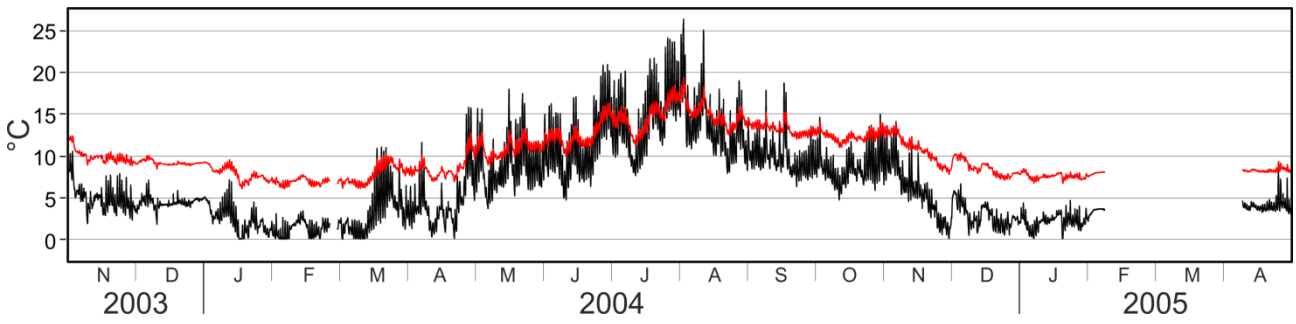

Figure 9 - Ambient temperature measured inside BVD station during late 2003 to early 2005. The black and red curves show, respectively, ambient temperatures outside and inside the polyurethane box hosting the gravity sensor.

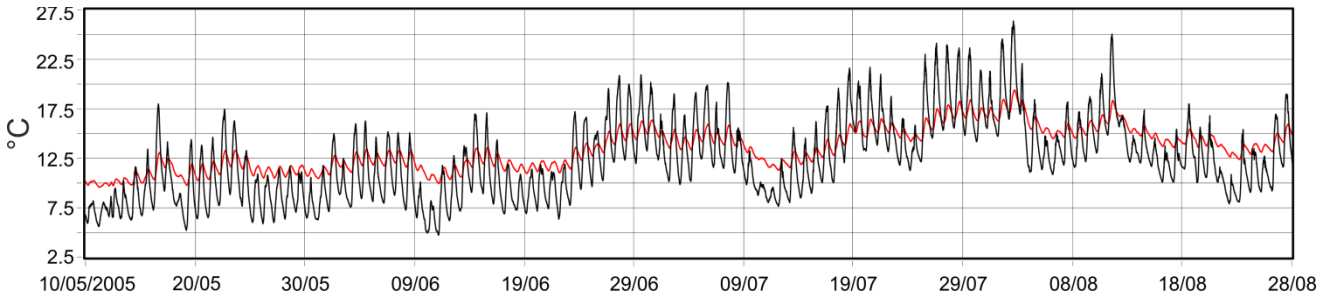

Figure 10 - 110-day sub-period of the time-series shown in Fig. 9. Daily changes in ambient temperature are up to ~10 and ~2°C, outside (black curve) and inside (red curve) the polyurethane box hosting the gravity sensor, respectively.

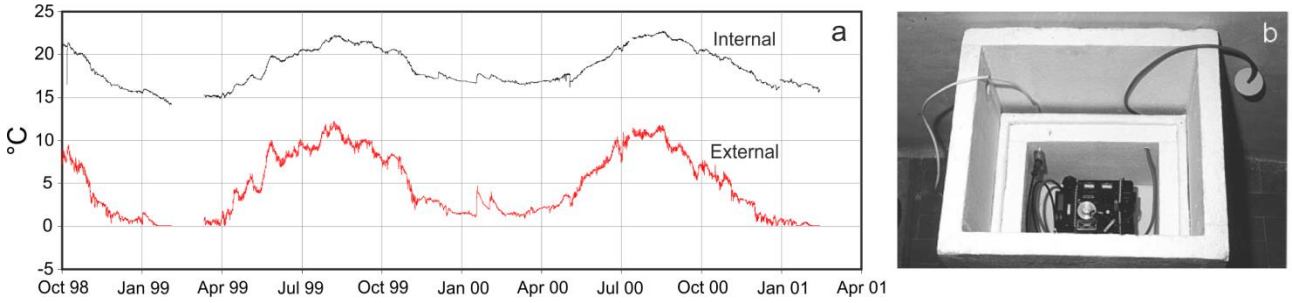

Figure 11 - a) Ambient temperature measured at PDN station, between late 1998 and early 2001. The red and black curves show, respectively, temperature outside and inside the thermally insulating box shown in (b).

Ambient temperature data were also collected inside the facilities of the Pizzi Deneri Volcanological Observatory (PDN, Fig. 3; northern slope, 2800 m elevation), where a continuously running station has been operating intermittently since the late 1990s. As reported by Carbone et al (2017), ambient temperature recorded at PDN, inside and outside (black and red curves, respectively, in Fig. 11) the thermally insulating polystyrene box hosting the gravimeter has a peak-to-peak amplitude of slightly more than 5°C and slightly more than 10°C, respectively. In this case, the seasonal component dominates the signal, while daily changes are almost completely filtered out by the building of the observatory.

The variability ranges of ambient temperatures observed at PDN can be regarded as a reference for the quantum gravimeter that will be produced and field-tested at Mt. Etna in the framework of NEWTON-g. Indeed, contrarily to MEMS devices that can be installed even in small protective boxes, this instrument requires some kind of hut or vault to house the instrumentation.

5. THE EFFECT OF GROUND SHAKING ON STANDARD GRAVIMETERS

Carbone et al (2015) showed that, during the paroxysmal stages of explosive activity at Mt. Etna, the severe ground shaking (volcanic tremor) may corrupt the gravity signal from continuously recording spring gravimeters to the extent of unintelligibility.

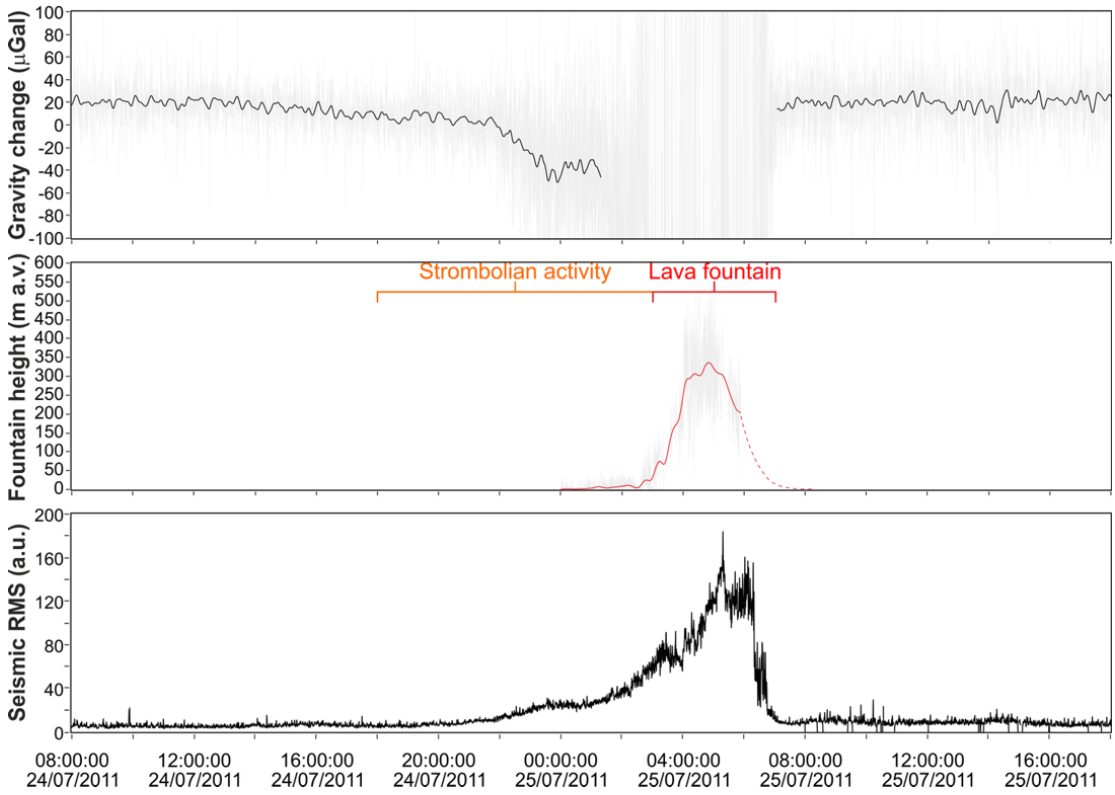

Figure 12 - From top to bottom: (i) gravity signal from a site within 1km of the summit craters of Etna, encompassing a fountaining episode, (ii) lava fountain height (meters above the vent) and (iii) RMS of seismic signal recorded by the vertical component of a summit station. The lacking filtered data (black curve) in the top graph indicates that data are disregarded due to critical "ground shaking conditions" (Modified from Carbone et al., 2015).

Indeed, during paroxysmal events, the amplitude of the volcanic tremor may increase by more than one order of magnitude (Fig. 12) and, because of resonance effects, the amplitude of the higher frequency component of the gravity signal (periods ranging from the sampling interval –usually 1sec– to several minutes) increases to more than 10 times higher than the amplitude of the expected gravity changes.

The signal from SGs is also affected by ground motion during phases of high volcanic tremor, mainly due to the horizontal forces from seismic shaking that push the proof superconducting sphere off to the side. Since the levitation force gets weaker as the sphere moves off the axis of the magnet coils, the sphere drops, thus simulating an increase in gravity (Warburton, pers. comm.).

In the light of the above observations, it is important to perform tests on the new devices that will be developed in the framework of NEWTON-g, aimed at understanding whether they can perform better than currently available gravimeters during phases of high tremor. Thanks to the deep knowledge of the spectral and amplitude characteristics of the volcanic tremor at Etna (e.g., Cannata et al., 2015), the above tests could be accomplished through the accurate simulation of the ground shacking during paroxysmal phases of the activity.

REFERENCES

Andò, B. and Carbone, D., 2004. A test on a Neuro-Fuzzy algorithm used to reduce continuous gravity records for the effect of meteorological parameters. Phys. Earth Planet. Inter. 142 (1–2), 37–47, doi:10.1016/j.pepi.2003.12.006.

Andò, B. and Carbone, D., 2006. A new computational approach to reduce the signal from continuously recording gravimeters for the effect of atmospheric temperature. Phys. Earth Planet. Inter., 159 (3–4), 247–256, doi:10.1016/j.pepi.2006.07.009.

Battaglia, M., Segall, P. and Roberts, C., 2003. The mechanics of unrest at Long Valley caldera, California. 2. Constraining the nature of the source using geodetic and micro-gravity data. J. Volcanol. Geotherm. Res. 127 (3-4), 219–245, doi:10.1016/S0377-0273(03)00171-9.

Bonforte, A., Bonaccorso A., Guglielmino, F., Palano M., and Puglisi G., 2008. Feeding system and magma storage beneath Mt. Etna as revealed by recent inflation/deflation cycles. J. Geophys. Res., 113, B05406, 10.1029/2007JB005334.

Branca, S., Carbone, D. and Greco, F., 2003. Intrusive mechanism of the 2002 NE-Rift eruption at Mt. Etna (Italy) inferred through continuous microgravity data and volcanological evidences. Geophys. Res. Lett. 30 (20), doi:10.1029/2003GL018250.

Budetta, G., Carbone, D., and Greco, F., 1999. Subsurface mass redistribution at Mount Etna (Italy) during the 1995–96 explosive activity detected by microgravity studies. Geophys. J. Int. 138 (1), 77–88, doi:10.1046/j.1365-246x.1999.00836.x.

Cannata, A. et al., 2015. Pressurization and depressurization phases inside the plumbing system of Mount Etna volcano: Evidence from a multiparametric approach. J. Geophys. Res. Solid Earth 120, 5965–5982, doi:10.1002/2015JB012227

Carbone, D. and Poland, M.P., 2012. Gravity fluctuations induced by magma convection at Kīlauea Volcano, Hawai'i. Geology, 40(9): 803-806, doi:10.1130/G33060.1.

Carbone, D., Budetta, G. and Greco, F., 2003c. Possible mechanisms of magma redistribution under Mt. Etna during the 1994 – 1999 period detected through microgravity measurements. Geophys. J. Int. 153 (1), 187–200, doi:10.1046/j.1365-246X.2003.01901.x

Carbone, D., Currenti, G. and Del Negro, C., 2008a. Multiobjective genetic algorithm inversion of ground deformation and gravity changes spanning the 1981 eruption of Etna volcano. J. Geophys. Res. 113 (7), doi:10.1029/2006JB004917.

Carbone, D., Zuccarello, L. and Saccorotti, G., 2008b. Geophysical indications of magma uprising at Mt Etna during the December 2005 to January 2006 non-eruptive period. Geophys. Res. Lett. 35 (6), doi:10.1029/2008GL033212.

Carbone, D., D'Amico, S., Musumeci, C. and Greco, F., 2009. Comparison between the 1994–2006 seismic and gravity data from Mt. Etna: New insight into the long-term behavior of a complex volcano. Earth Planet. Sci. Lett. 279 (3–4), 282–292, doi:10.1016/j.epsl.2009.01.007.

Carbone, D., Aloisi, M., Vinciguerra, S. and Puglisi, G., 2014. Stress, strain and mass changes at Mt. Etna during the period between the 1991–93 and 2001 flank eruptions. Earth Sci. Rev. 138, 454–468, doi:10.1016/j.earscirev.2014.07.004.

Carbone, D., Zuccarello, L., Messina, A., Scollo, S. and Rymer, H., 2015. Balancing bulk gas accumulation and gas output before and during lava fountaining episodes at Mt. Etna. Sci. Rep. 5, 18049, doi:10.1038/srep18049.

Carbone, D., Poland, M. P., Diament, M. and Greco, F., 2017. The added value of time-variable microgravimetry to the understanding of how volcanoes work. Earth Sci. Rev. 169, 146-179, doi: 10.1016/j.earscirev.2017.04.014.

Creutzfeldt, B., Güntner , A., Klügel, T., and Wziontek, H., 2008. Simulating the influence of water storage changes on the superconducting gravimeter of the Geodetic Observatory Wettzell, Germany., Geophysics, 73, WA95-WA104.

Crossley, D., Xu, S., Van Dam, T., 1998. Comprehensive analysis of 2 years of SG data from Table Mountain, Colorado. Proc. 13th Int. Symp. Earth Tides, Brussels, pp. 659–668.

Furuya, M., Okubo, S., Kimata, F., Miyajima, R., Meilano, I., Sun, W., Tanaka, Y. and Miyazaki, T., 2003a. Mass budget of the magma flow in the 2000 volcano-seismic activity at Izu-islands, Japan. Earth, Planets, and Space 55 (7), 375–385, doi:10.1186/BF03351771.

Furuya, M., Okubo, S., Sun, W., Tanaka, Y., Oikawa, J., Watanabe, H., and Maekawa, T., 2003b. Spatiotemporal gravity changes at Miyakejima Volcano, Japan: Caldera collapse, explosive eruptions and magma movement. J. Geophys. Res., 108, 2219, doi: 10.1029/2002JB001989, B4.

Hemmings, B., Gottsmann, J., Whitaker, F. and Coco, A., 2016. Investigating hydrological contributions to volcano monitoring signals. A time-lapse gravity example. Geophys. J. Int. 207(1), 259-273, doi: 10.1093/gji/ggw266.

Ménoret, V., Vermeulen, P., Le Moigne, N., Bonvalot, S., Bouyer, P., Landragin, A., Desruelle, B., 2018. Gravity measurements below 10−9 g with a transportable absolute quantum gravimeter. Sci. Rep. 8, 12300, doi: 10.1038/s41598-018-30608-1DO

Middlemiss, R.P., Samarelli, A., Paul, D.J., Hough, J., Rowan, S. and Hammond, G.D., 2016. Measurement of the Earth tides with a MEMS gravimeter. Nature 531 (7596), 614–617, doi:10.1038/nature17397.

Segall, P., 2010. Earthquake and Volcano Deformation. Princeton University Press: Princeton. 465 pp.